Plectoneme creation reduces the rotational friction of a polymer

H. Wada[1] and R. R. Netz[2]

[1] *Yukawa Institute for Theoretical Physics, Kyoto University, Kyoto 606-8502, Japan*
[2] *Department of Physics, Technical University Munich, 85748 Garching, Germany*

PACS 87.15.H- – Dynamics of biomolecules
PACS 87.16.Ka – Filaments, microtubules, their networks, and supramolecular assemblies
PACS 47.15.G- – Low-Reynolds-number (creeping) flows

Abstract. - The torsional dynamics of a semiflexible polymer with a contour length L larger than its persistence length L_p that is rotated at fixed frequency ω_0 at one end is studied by scaling arguments and hydrodynamic simulations. We find a non-equilibrium transition at a critical frequency ω_*: In the linear regime, $\omega_0 < \omega_*$, axial spinning is the dominant dissipation mode. In the non-linear regime, $\omega_0 > \omega_*$, the twist-dissipation mode involves the continuous creation of plectonemes close to the driven end and the rotational friction is substantially reduced.

Introduction. – The properties of semiflexible polymers have received continuous interest and attention from biophysicists for the last two decades. This is so since they constitute a minimal yet realistic mechanical model for biological macromolecules such as DNA and filamentous proteins. The framework of statistical mechanics provides various equilibrium properties of semiflexible polymers such as the force-extension relationship [1], which have been successfully tested through detailed comparison with experimental data obtained from newly developed micromanipulation techniques employing optical tweezers and magnetic beads [2]. The importance of torsional elasticity has been recognized in the context of DNA supercoiling [3]. Driven by experiments where both stretching and twist of single biopolymers could be controlled [4], theories were generalized to include twisting effects as well and provide quantitative agreement on the static level [5].

The in-vivo functioning of DNA involves non-equilibrium dynamic twist effects that mostly have to do with the activity of various DNA-processing proteins [6]. For example, in replication, the process by which a DNA chain is duplicated into two identical daughter strands, the helical nature of DNA requires daughter strands to unwind and thus the mother strand to rotate around its axis. This large scale motion has been considered a conceptual obstacle; it was resolved by a simple calculation demonstrating that the friction dissipation associated with simple axial-spinning of DNA (like in a speedometer cable) is rather small compared to typical biological free energies [7]. In transcription, the process by which the DNA informational content is copied into a continuously growing RNA chain, it was suggested that a long nascent RNA chain might (either due to its own hydrodynamic friction or via anchoring to some other cellular component) provide enough rotational resistance to force the DNA strand to rotate around its own axis [8]. Experimental in-vivo and in-vitro studies found large degrees of DNA supercoiling upon transcription, being positive in front and negative behind the transcriptional complex [8]. This finding, however, is at odds with the above-mentioned simple axial-spinning scenario [7], since the rotational friction of bare DNA seems not large enough to induce sufficient torsional stress needed to induce supercoiling [9]. In an effort to reconcile the conflicting experimental results, Nelson introduced the notion of static bends along DNA, which substantially increase the rotational friction [9]. So far, the issue of the rotational friction of a semiflexible chain is still a matter of interest and debate. Single-molecule experiments on rotating DNA failed to observe the static-bend-induced anomaly of the rotational friction, but this could possibly be related to the high rotational frequency employed in the experiments [10]. Several studies did not provide a clear-cut answer as to what the influence of static DNA bends is and whether other factors present in in-vivo studies are needed to induce substantial supercoiling of DNA under twist injection [11–14].

In this Letter we use non-equilibrium scaling arguments and hydrodynamic simulations and consider a fundamental scenario, namely a homogeneous semiflexible polymer in the stationary limit, that is axially rotated at one end

at frequency ω_0 with the other end free, as schematically depicted in Fig. 1. In the absence of shape fluctuations, i.e. at zero temperature, an elasto-hydrodynamic instability occurs at a critical driving frequency ω_c that separates a twirling from a whirling regime [15]; for $\omega_0 < \omega_c$ the rod stays straight and undergoes simple axial spinning (twirling), while for $\omega_0 > \omega_c$ the rod buckles and displays a combination of axial spinning and rigid-body rotation (whirling). Including thermal effects, elastic shape fluctuations of the rod round off the transition and shift the instability to lower frequency [16]. In the present study, we consider the opposite limit where the chain contour length is much larger than bend and twist persistence lengths and the twirling-whirling instability is completely washed out by thermal fluctuations. This is relevant to transcription-driven DNA supercoiling, but has not been studied as an elasto-hydrodynamic problem for a homogenous semiflexible chain before. As our main result, we find in addition to the well-known axial-spinning regime, realized for low driving frequency $\omega_0 < \omega_*$, a novel plectoneme dominated regime at high frequencies $\omega_0 > \omega_*$. In this regime, twist is converted locally into writhe (in the form of plectonemes) close to the driven end and then diffuses out to the free end. For sufficiently long chains, the crossover frequency ω_* is much larger than the twirling-whirling threshold ω_c. Quite surprisingly, in the plectoneme regime the overall rotational friction is significantly reduced as compared to the axial-spinning scenario, i.e., the plectoneme dissipation channel transforms the injected twist into writhing motion at very low frictional cost. This mechanism could be biologically relevant since it shows how transcription might produce positively super-coiled DNA structures that could favorably interact with negatively super-coiled nucleosomal structure ahead of the RNA polymerase [6] even in topologically open systems and at very small energy expenditure.

Model. – Within linear elasticity theory, the elastic energy of an isotropic rod of contour length L is given by

$$E_{el} = \int_0^L ds \left[\frac{A}{2}\kappa(s)^2 + \frac{C}{2}\Omega(s)^2\right], \qquad (1)$$

where A and C are the bend and twist rigidities, $\kappa(s) = |\partial_s^2 \mathbf{r}|$ is the local curvature with $\mathbf{r}(s)$ the position of the rod centerline and ∂_s denoting the derivative with respect to the arclength s. The local twist density $\Omega(s)$ is defined by $\Omega(s) = \partial_s \phi(s)$ where ϕ is the rotational angle about the local tangent $\partial_s \mathbf{r}$. Note that Ω in eq. (1) includes also the twist contribution due to geometric torsion, i.e. changes of $\phi(s)$ are also generated e.g. by out-of-plane bending [17,18].

In our simulations, a filament is modelled as a chain of $N+1$ connected spheres of diameter a. The total energy of the system, $E = E_{st} + E_{el} + E_{LJ}$, includes a stretching contribution ensuring connectivity of spheres, $E_{st} = K/2 \sum_{j=1}^{N} (|\mathbf{r}_{j+1} - \mathbf{r}_j| - a)^2$, where $\mathbf{r}_j$ is the position vector of monomer j, and a truncated Lennard-Jones potential to account for chain self-avoidance, where $E_{LJ} = \epsilon_{LJ} \sum_{i<j} [(a/r_{ij})^{12} - 2(a/r_{ij})^6]$ applied only for $r_{ij} = |\mathbf{r}_i - \mathbf{r}_j| < a$. The local elastic translational force $\mathbf{F}_j$ and torque about the local tangent T_j acting on each sphere are calculated using the variational method described previously [18], leading to the coupled Langevin equations: $\partial_t \mathbf{r}_i = \sum_{j=1}^{N+1} \boldsymbol{\mu}_{ij} \cdot \mathbf{F}_j + \boldsymbol{\xi}_i(t)$ and $\partial_t \phi_i = (\pi \eta a^3)^{-1} T_i + \Xi_i(t)$, where ϕ_i is the rotation angle around the bond vector $\mathbf{r}_{i+1} - \mathbf{r}_i$. Hydrodynamic interactions between two spheres i and j are included via the Rotne-Prager mobility tensor $\boldsymbol{\mu}_{ij}$ [19]. For the translational self-mobility of the spherical monomers with diameter a we use the standard Stokes formula $\boldsymbol{\mu}_{ii} = \mathbf{1}/(3\pi\eta a) \equiv \mu_0 \mathbf{1}$. The vectorial random displacements $\boldsymbol{\xi}(t)$ and $\Xi(t)$ model the coupling to a heat bath and obey the fluctuation-dissipation relations implemented numerically by a Cholesky factorization [19]. For the numerical integrations we discretize the Langevin equations with a time step Δ and rescale all lengths, times and energies, leading to the dimensionless parameter $\tilde{\Delta} = \Delta k_B T \mu_0 / a^2$. We set the twist-bend rigidity ratio to $C/A = 1$ and the stretching modulus to $K/k_B T a^2 = 10^3$, which gives negligible bond length fluctuations. The self-crossing of the chain is entirely prevented by setting $\epsilon_{LJ}/k_B T = 10$. For sufficient numerical accuracy we choose a time step $\tilde{\Delta} = 0.0004$. Output values are calculated every 10^3-10^4 steps, total simulation times are 10^7 steps, the first 10^6 steps are not

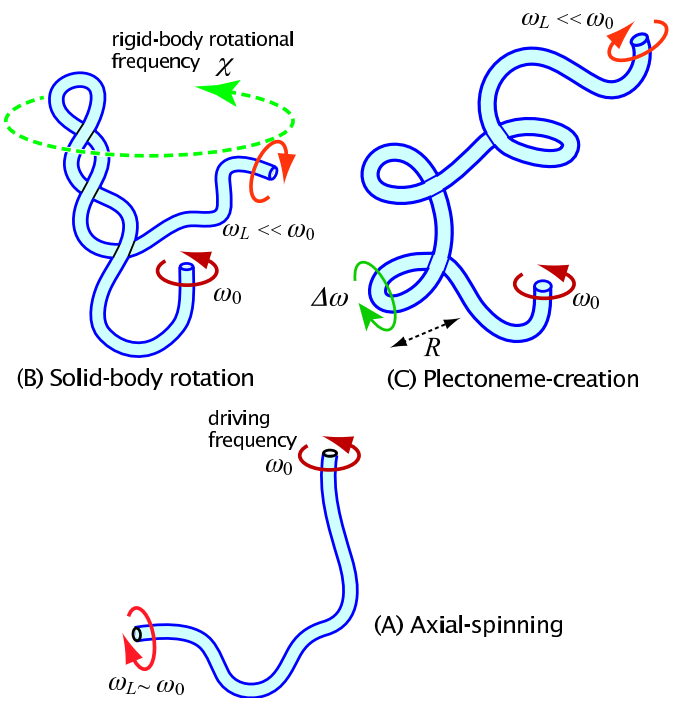

Fig. 1: A semiflexible polymer is rotated at frequency ω_0 at a fixed end and exhibits rotation at frequency ω_L at its free end. The three twist-dissipation channels are (A) axial-spinning, (B) solid-body rotation, and (C) plectoneme-creation.

included in the data analysis. The boundary condition at the forced end, $\partial_s \mathbf{r}(0) = \hat{\mathbf{z}}$, is realized by fixing the first two monomers in space by applying virtual forces, which also act (via the mobility tensor) on the rest of the filament. The rotational driving at the base imposes $\partial_t \phi_1 = \omega_0$, while force- and torque-free boundary conditions are adopted for the other end. The number of beads is in the range $L/a = N = 30 - 100$. Throughout this study, the persistence length is set to $L_p = 10a$, thus $L/L_p = 3 - 10$.

Buckling and plectonemes. – To set the stage, we first repeat the zero-temperature scaling argument for the critical frequency ω_c at which an axially rotated rod exhibits the buckling instability. At low rotational frequency, $\omega_0 < \omega_c$, the rod is twisted but remains straight and the torque at the base balances the total rotational drag, $\pi\eta a^2 \omega_0 L \sim C\Omega(0)$. On the scaling level, the rod buckles when the twisting torque, $C\Omega(0)$, becomes comparable to the bending torque, A/L, giving the critical frequency $\omega_c \sim A/(\pi\eta a^2 L^2)$ independent of the twist rigidity C [15]. The linear stability analysis predicts an instability at $\omega_c \equiv 8.9A/(\pi\eta a^2 L^2)$ [15], the numerical prefactor was confirmed by simulations in the zero-temperature-limit, i.e. for a very stiff polymer with persistence length $L_p = A/k_B T \gg L$ [16]. In Fig. 2 we show typical chain snapshots obtained in our dynamic simulations for driving frequencies $\omega_0/\omega_c = 0.3$, 15 and 40 for a rather flexible chain with $L/L_p = 10$. For $\omega_0 < \omega_c$, the chain flexes randomly due to thermal motions and spins about its local axis at frequency $\sim \omega_0$. For $\omega_0 \gg \omega_c$, in contrast, the polymer exhibits continuous generation of plectoneme-like structures and their diffusive transport from the driving end to the free end. In the following we present a much-simplified scaling theory, valid for long elastic rods $L \gg L_p$, that establishes a minimal framework for treating the competitive twist transport due to axial spinning and plectoneme creation.

Scaling. – There are three different ways for the polymer to transport the injected twist to its free end, see fig. 1. The first one is the (A) axial spinning mode, where the polymer rotates around its contour like a speedometer cable, which we show to be the dominant dissipation mode for low enough driving frequencies. The second one is the (B) solid-body rotation mode, where the whole polymer coil whirls around the rotational axis at some frequency χ. The third one is the (C) plectoneme creation/diffusion mode, in which plectoneme-like structures are continuously generated at the rotated end and are transported diffusively towards the free end. As we show in this paper, this dynamic twist-writhe conversion is a highly nonlinear mechanism that provides a very efficient means of relieving torsional stress at elevated driving frequencies. Noting that in a stationary state, the twist that is injected into the polymer, ω_0, has to exit the chain at the free end either in the form of axial spinning, solid-body rotation of

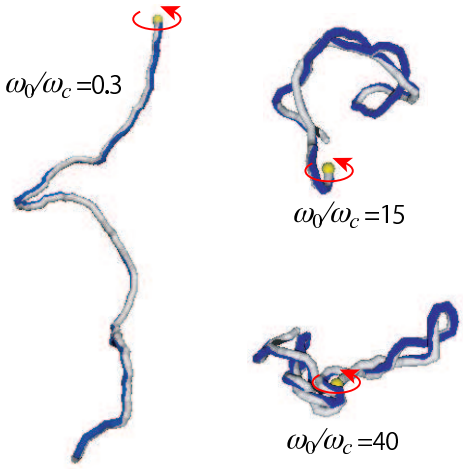

Fig. 2: Typical chain conformations from our hydrodynamic simulations for chain length $L = 100a$ and persistence length $L_p = 10a$ and rotational frequency $\omega_0/\omega_c = 0.3, 15$ and 40.

frequency χ, or writhe, we write

$$\omega_0 \quad = \quad \omega_L + \chi + \Delta\omega, \tag{2}$$

where ω_L is the axial spinning frequency of the free end and $\Delta\omega$ denotes the fraction that is converted into writhe. In order to decide which of these three channels is in fact realized, we use the concept of minimum entropy production for non-equilibrium stationary states [20], according to which the state of least dissipation is stable. We will later confirm each of our scaling results by our simulations, which gives further credibility to our scaling approach. We thus have to estimate the power dissipation in each of the modes depicted in fig. 1. The power dissipation due to axial spinning is $P_{as} \sim \eta L a^2 \omega_L^2$. Here we assume that average axial spinning frequency is ω_L, meaning that in the plectoneme regime the rotational profile $\omega(s)$ decays very quickly (in fact exponentially) along the chain contour to the value $\sim \omega_L$. This is confirmed by our simulations, see fig. 4 (b). Likewise, the power dissipation due to solid-body rotation is given as $P_{sb} \sim \eta R^3 \chi^2$. Except for a compact globule with $R^3 \sim a^2 L$ we see that axial spinning is a less costly channel for twist transport than solid-body rotation, i.e. $P_{as} \ll P_{sb}$. We therefore neglect solid-body rotation in what follows. The plectoneme-creation channel is more complicated. We consider the creation of a single loop of radius R nearby the driven end, see fig. 1 (C). Extension to a more complex plectoneme structure involving multi-loops (as actually observed in the simulations, see fig. 2) is straightforward, but does not change the conclusions on the scaling level. The bending energy of one loop is $k_B T L_p/R$, the loop creation frequency is $\Delta\omega$, thus the power consumption is $P_{loop} \sim k_B T \Delta\omega L_p/R$. In order to generate a loop of radius R nearby the driven end, the whole chain has to slide by the excess length $2\pi R$ during the time scale of $(\Delta\omega)^{-1}$. The frictional

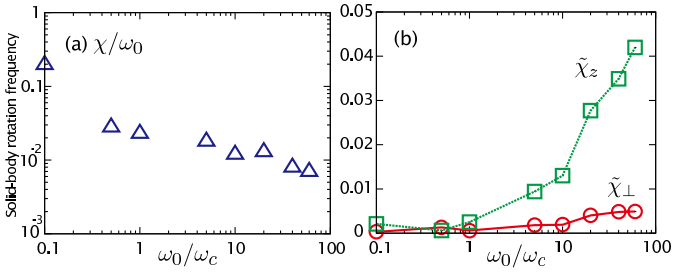

Fig. 3: (a) Relative solid-body rotation frequency, χ/ω_0, as a function of ω_0/ω_c. (b) Rescaled components of the vector $\boldsymbol{\chi}$, $\tilde{\chi}_\perp = \chi_\perp a^2/(\mu_0 k_B T)$, and $\tilde{\chi}_z = \chi_z a^2/(\mu_0 k_B T)$, as a function of ω_0/ω_c. Note that $\chi = (\chi_\perp^2 + \chi_z^2)^{1/2}$. The data are obtained for $L = 50a$ and $L_p = 10a$.

force associated with this sliding with velocity $\sim R\Delta\omega$ is $F_{slide} \sim \eta L R\Delta\omega/\ln(L/a)$. Neglecting the logarithmic hydrodynamic correction, the power dissipation of sliding is $P_{slide} \sim F_{slide} R\Delta\omega \sim \eta L(R\Delta\omega)^2$. Minimizing the total plectoneme creation dissipation, $P_{plec} = P_{loop} + P_{slide}$, with respect to the loop radius R, we obtain

$$P_{plec} \sim (k_B T L_p \Delta\omega)^{4/3} (\eta L)^{1/3}, \quad (3)$$

with the loop size given by $R^3 \sim k_B T L_p/(\eta L\Delta\omega)$. Due to the fractional power law $P_{plec} \sim (\Delta\omega)^{4/3}$, it is easy to see that plectoneme creation is unfavorable at low frequencies but will win over axial spinning at high frequencies. We now minimize the total dissipation $P \sim P_{as} + P_{plec}$ with respect to the unknown frequency at the free end, ω_L, and use eq. (2) and $\chi = 0$. For low frequency we obtain pure axial spinning, $\omega_L \sim \omega_0$, i.e. the twist that is injected at one end comes out as axial spinning at the other end. For high frequencies $\omega_0 > \omega_*$, with a crossover frequency defined as

$$\omega_* \equiv k_B T L_p/(\pi\eta a^3 L) \sim \omega_c (L/a), \quad (4)$$

on the other hand, we obtain

$$\omega_L \sim \omega_*^{2/3} \omega_0^{1/3}, \quad (5)$$

$$P \sim \eta L a^2 \omega_*^{2/3} \omega_0^{4/3}. \quad (6)$$

Interestingly, the cross-over frequency ω_* is much larger than the zero-temperature twirling-whirling critical frequency ω_c by a factor proportional to the chain contour length, L/a, and the dissipation P is reduced compared to the axial spinning scenario P_{as}.

To confirm these predictions, we extract the solid-body rotation rate vector, $\boldsymbol{\chi}$, from our hydrodynamic simulations. For rigid-body rotation, i.e, $\partial_t \mathbf{r} \simeq \boldsymbol{\chi} \times \mathbf{r}$, we obtain the vector $\boldsymbol{\chi} = (\chi_\perp, \chi_z)$ via $\boldsymbol{\chi} = \mathbf{I}^{-1} \cdot \mathbf{L}$, where $\mathbf{I} = \sum_{j=1}^N [\mathbf{r}_j \mathbf{1} - \mathbf{r}_j \mathbf{r}_j]$ is the moment of inertia tensor and $\mathbf{L} = \sum_{j=1}^N \mathbf{r} \times d\mathbf{r}/dt$ is the polymer angular momentum (the mass of the polymer beads is set to unity). Fig. 3b) shows $\boldsymbol{\chi} = (\chi_\perp, \chi_z)$ as a function of the rescaled driving frequency, ω_0/ω_c; solid-body rotation is small for $\omega_0 < \omega_c$, while χ_z grows significantly beyond ω_c. The hydrodynamic shear due to this rotation deforms the plectonemes at high values of ω_0, which is a secondary effect that we neglect in the current version of our scaling arguments. In fig. 3 (a), we show that $\chi/\omega_0 = |\boldsymbol{\chi}|/\omega_0$ is much smaller than unity, which confirms that solid-body rotation is negligible compared to other dissipation channels.

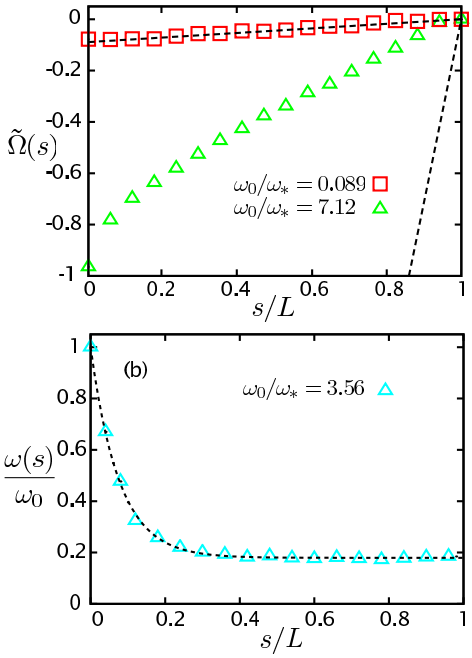

Fig. 4: (a) Steady-state profile of the rescaled twist density, $\tilde{\Omega}(s) = \Omega(s)a$, for two different driving frequencies, $\omega_0/\omega_* = 0.089$ (squares) and 7.12 (triangles). The broken lines are the prediction from linearized theory, see text. (b) Steady-state profile of the rescaled rotational velocity, $\omega(s)/\omega_0$ together with an exponential fit (broken line), for $\omega_0/\omega_* = 3.56$. All data were obtained for $L = 50a$ and $L_p = 10a$.

The total twist Tw is defined as the integrated twist density along the chain arclength, $Tw = (2\pi)^{-1} \int_0^L ds\Omega(s)$. In the axial-spinning regime, i.e., $\omega_0 < \omega_*$, chain shape fluctuations are decoupled from twisting motion, and the injected twist propagates diffusively along the chain [9]. The twist Ω thus obeys the linear diffusion equation, $\pi\eta a^2 \partial_t \Omega = C\partial_s^2 \Omega$. In steady state under the boundary condition, $C\Omega(0) = \pi\eta a^2 \omega_0 L$, we thus obtain $\Omega(s) = (\pi\eta a^2 \omega_0/C)(s - L)$. This is in quantitative agreement with simulation for $\omega_0/\omega_* = 0.089$, as seen in fig. 4 (a) (open squares and broken line). The total twist in this regime is given by $Tw \simeq -\pi\eta a^2 \omega_0 L^2/(4\pi C) = -(A/4\pi C)(L/a)(\omega_0/\omega_*)$ and thus is linear in the driving frequency ω_0. In the plectoneme regime, on the other hand, the twist is much reduced compared to the linear law (lower broken line in fig. 4 (a)) and shows a nonlin-

ear spatial profile (open triangles in fig. 4 (a)). In this regime, the twist density Ω receives an additional contribution from the geometric torsion due to plectoneme formation, which however we neglect. Assuming the twist to be proportional to the average spinning frequency ω_L in the region where plectonemes have already formed, i.e. $Tw \sim (AL/aC)(\omega_L/\omega_*) \sim (\omega_0/\omega_*)^{1/3}$, we thus predict

$$Tw \sim \begin{cases} \frac{AL}{4\pi aC}\frac{\omega_0}{\omega_*} & (\omega_0 < \omega_*) \\ \frac{AL}{aC}\left(\frac{\omega_0}{\omega_*}\right)^{1/3} & (\omega_0 > \omega_*). \end{cases} \quad (7)$$

Finally, the effective rotational friction coefficient Γ_r is defined via $P \sim \Gamma_r \omega_0^2$, where P is the total dissipation, given by eq. (6) in the plectoneme regime. We obtain

$$\frac{\Gamma_r}{\pi\eta a^2 L} \sim \begin{cases} 1 & (\omega_0 < \omega_*) \\ \left(\frac{\omega_0}{\omega_*}\right)^{-2/3} & (\omega_0 > \omega_*). \end{cases} \quad (8)$$

For $\omega_0 < \omega_*$, the rotational friction corresponds to the axial spinning scenario, while for $\omega_0 > \omega_*$ a drastic decrease is predicted. Note that for $\omega_0 > \omega_*$ the dependence on chain length is $\Gamma_r \sim \omega_0^{-2/3} L^{1/3}$ and thus increases only sub-linearly with polymer length.

In Fig. 5, ω_L, Tw and Γ_r from simulations are plotted as a function of ω_0/ω_* and confirm the analytical predictions for the non-linear plectoneme regime , eqs. (5), (7) and (8). In the simulations, the torque M_0 at a given driving frequency ω_0 is measured and averaged to obtain $\Gamma_r = \langle M_0 \rangle / \omega_0$. In particular, the crossover frequency between the axial-spinning and the plectoneme regime is quite consistently found to occur at $\omega_0 = c_* \omega_* \sim (L/a)\omega_c$ with $c_* = 0.4 \pm 0.1$ and ω_* defined in eq. (4). Note that the whirling instability, at $\omega_0 \simeq \omega_c$ and realized only for $L/L_p < 1$, is conceptually distinct from the plectoneme transition at $\omega_0 \simeq \omega_*$, which is only observable for long chains $L/L_p \gg 1$. In fact, the two transitions do not merge or interconnect at intermediate values of L/L_p: for $L/L_p \simeq 1$ a semiflexible chain rather shows a continuous shape and rotational mode evolution with increasing ω_0 without a sharply defined transition.

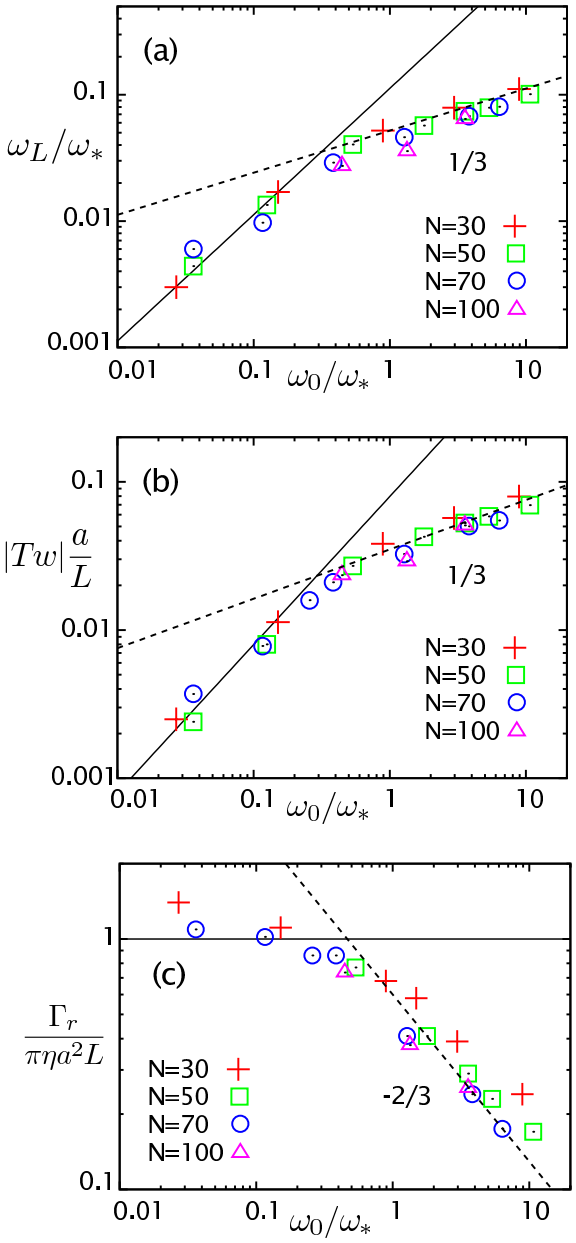

Fig. 5: Scaling plots of hydrodynamic simulation results. (a) Rescaled axial spinning frequency at free end, ω_L/ω_*, (b) total twist divided by the chain length, $|Tw|(a/L)$), and (c) rescaled rotational friction constant, $\Gamma_r/(\pi\eta a^2 L)$, plotted as a function of ω_0/ω_*. Soild lines denote the predictions from linear theory in the axial spinning regime valid for $\omega_0 < \omega_*$, broken lines denote the non-linear results valid in the plectoneme regime as given in eqs. (5), (7) and (8). The crossover between the regimes occurs around a value of $\omega_0 = c_* \omega_*$ with $c_* = 0.4 \pm 0.1$.

Discussion. – For a hydrodynamic diameter of ds-DNA of $a \sim 2$ nm, a bend persistence length $L_p \sim 30$ nm and length $L \sim 12\mu$m, we obtain according to eq. (4) a cross over frequency $c_* \omega_* \sim 2 \times 10^5$ rad/s. The rotational friction of DNA molecules of length $L \sim 12$ μm has been measured for rotational frequencies up to $\omega_0 \sim 12000$ rad/s in DNA unzipping experiments [10] and showed no detectable non-linear frequency dependence, in agreement with our estimate for the threshold ω_*. On the other hand, for longer chains or in a crowded cellular environment with a much elevated viscosity, the crossover frequency ω_* can be lowered to an experimentally reachable value. The critical torque $M_* = \pi\eta a^2 L c_* \omega_* \simeq c_* \pi k_B T L_p / a$ is independent of both viscosity and chain length and for bare DNA is of the order of a few tens of $k_B T$, too high for, e.g., single *Escherichia coli* RNA polymerase to achieve. But for chromatin structures, the effective bending persistence length L_p^{chrom} has been shown to stay rather constant while the

effective radius a^{chrom} is increased substantially [6], meaning that the critical torque M_*^{chrom} for a chromatin fiber might be of the order of k_BT, quite in reach of typical torques generated by polymerase.

In recent experiments, the elongation dynamics of supercoiled DNA in response to sudden increase of tension was studied [14]. The dynamics showed almost no effect of the continuous removal of plectonemes, setting an upper bound on the hydrodynamic friction associated with DNA rotation, which turns out to be in agreement with the axial spinning scenario and thus is consistent with our results. Previous *in vitro* and *in vivo* studies on transcriptionally-driven DNA supercoiling have been interpreted as evidence of enhanced rotational friction when compared to the simple axial-spinning estimate [8]. Krebs and Dunaway showed *in vivo* that polymerase drives DNA supercoiling during the transcription process for linear DNA templates longer than 17 to 19 kbp [11]. One explanation involves static DNA bends or kinks stabilized by DNA-binding proteins, which are suggested to significantly slow down the torsional relaxation and lead to a considerably enhanced rotational drag torque [9, 12, 13]. It remains to study how static DNA bends interfere with the plectoneme creation/diffusion scenario developed in this paper.

To summarize, using scaling arguments and hydrodynamic simulations, we have studied the stationary nonequilibrium dynamics of torsionally driven semiflexible polymers. For chains much longer than their persistence length, $L > L_p$, two dynamical regimes are distinguished: for small driving frequency, $\omega_0 < \omega_*$, we find the standard axial-spinning regime where the chain flexes randomly and spins about its local axis. For large rotational frequency, $\omega_0 > \omega_*$, twist is locally converted into writhe close to the driven end and then diffuses out to the free end without much concerted solid-body rotation. In this plectoneme regime the filament exhibits only minimal axial spinning and a significant reduction of the rotational friction as compared to axial spinning is obtained. Two further conclusions might be biologically relevant: The nature of the twist-writhe conversion process leads to a narrow spatial localization of the twist density close to the rotated part of the chain, which in-vivo might guide and concentrate the activity of twist-sensitive proteins to a region close to the polymerase complex. Finally, the positive supercoiling, created in front of the point of twist-injection in the form of plectonemes, would be a simple physical mechanism for loosening or even driving off histones from their nucleosomale core particles, the negative supercoiling behind the twist-injection point would form a template for strengthening or reforming the nucleosomal core structure.

* * *

We thank C. Lavelle and P. Nelson for useful comments. Financial support from MEXT-Japan (Grant in Aid, No.20740241) and the Excellence Cluster Nano-Initiative-Munich is acknowledged.

REFERENCES

[1] Vologodskii A, *Macromolecules*, **27** (1994) 5623; Marko J. F., and Siggia E. D., *Macromolecules*, **28** (1995) 8759; Hallatschek O., Frey E. and Kroy K., *Phys. Rev. E*, **75** (2007) 031905.

[2] Ritort F, *J. Phys.: Condens. Matter.*, **18** (2006) R531 and references therein.

[3] Marko J. F. and Siggia E. D., *Phys. Rev. E*, **52** (1995) 2912.

[4] Strick T. R., Allemand J.-F., Bensimon D., Bensimon A. and Croquette V., *Science*, **271** (1996) 1835.

[5] Marko J. F., *Phys. Rev. E*, **55** (1997) 1758; Vologodskii A. V. and Marko J.F., *Biophys. J.*, **73** (1997) 123; Moroz J. D. and Nelson P., *Proc. Nat. Acad. Sci. USA*, **94** (1997) 14418.

[6] Lavelle C., *Biochem. Cell. Biol.*, **87** (2009) 307.

[7] Levinthal C. and Crane H., *Proc. Natl. Acad. Sci. U.S.A.*, **42** (1956) 436.

[8] Liu L. F. and Wang J. D., *Proc. Natl. Acad. Sci. U.S.A.*, **84** (1987) 7024; Tsao Y.-P., Wu H.-Y. and Liu L. F., *Cell*, **56** (1989) 111; Droge P. and Nordheim A., *Nucleic Acids Research*, **19** (1991) 2941.

[9] Nelson P., *Proc. Natl. Acad. Sci. U.S.A.*, **96** (1999) 14342.

[10] Thomen P., Bockelmann U. and Heslot F., *Phys. Rev. Lett.*, **88** (2002) 248102; Nelson P., *Phys. Rev. Lett.*, **92** (2004) 159801; Thomen P. and Heslot F., *Phys. Rev. Lett.*, **92** (2004) 159802.

[11] Krebs J. E. and Dunaway M., *Mol. Cell. Biol.*, **16** (1996) 5821.

[12] Leng F. and McMacken R., *Proc. Natl. Acad. Sci. U.S.A.*, **99** (2002) 9139; Leng F., Amado L. and McMacken R., *J. Biol. Chem.*, **279** (2004) 47564.

[13] Stupina V. A. and Wang J. C., *Proc. Natl. Acad. Sci. U.S.A*, **101** (2004) 8608.

[14] Crut A., Koster D. A., Seidel R., Wiggins C. H. and Dekker N. H., *Proc. Natl. Acad. Sci. U.S.A.*, **104** (2007) 11957.

[15] Wolgemuth C. W., Powers T. R. and Goldstein R. E., *Phys. Rev. Lett.*, **84** (2000) 1623.

[16] Wada H. and Netz R. R., *Europhys. Lett.*, **75** (2006) 645.

[17] Kamien R. D., *Eur. Phys. J. B*, **1** (1998) 1; Goldstein R. E., Powers T. R. and Wiggins C. H., *Phys. Rev. Lett.*, **80** (1998) 5232.

[18] Chirico G. and Langowski J., *Biopolymers*, **34** (1994) 415.

[19] Ermak D. L. and McCammon J. A., *J. Chem. Phys.*, **69** (1978) 1352.

[20] de Groot S. R. and Mazur P., *Non-equilibrium Thermodynamics* (North-Holland Publishing Co., Amsterdam) 1962, see Chap. V.